High-Throughput Microporous Tube-in-Tube Microreactor as Novel Gas–Liquid Contactor: Mass Transfer Study

Jian-Feng Chen
Key Lab for Nanomaterials, Ministry of Education, Chemical Engineering Dept, Beijing University of Chemical Technology, Beijing, 100029, PR China

Research Center of the Ministry of Education for High Gravity Engineering and Technology, Chemical Engineering Dept, Beijing University of Chemical Technology, Beijing, 100029, PR China

Gui-Zi Chen and Jie-Xin Wang
Key Lab for Nanomaterials, Ministry of Education, Chemical Engineering Dept, Beijing University of Chemical Technology, Beijing, 100029, PR China

Lei Shao
Research Center of the Ministry of Education for High Gravity Engineering and Technology, Chemical Engineering Dept, Beijing University of Chemical Technology, Beijing, 100029, PR China

Peng-Fei Li
Key Lab for Nanomaterials, Ministry of Education, Chemical Engineering Dept, Beijing University of Chemical Technology, Beijing, 100029, PR China

DOI 10.1002/aic.12260
Published online April 28, 2010 in Wiley Online Library (wileyonlinelibrary.com).

High-throughput microporous tube-in-tube microchannel reactor (MTMCR) was first designed and developed as a novel gas–liquid contactor. Experimentally measured $k_L\alpha$ *in MTMCR is at least one or two orders of magnitude higher than those in the conventional gas–liquid contactors. A high throughput of 500 L/h for gas and 43.31 L/h for liquid is over 60 times higher than that of T-type microchannel. An increase of the gas or liquid flow rate, as well as a reduction of the micropore size and annular channel width of MTMCR, could greatly intensify the gas–liquid mass transfer. The interfacial area,* α*, in MTMCR was measured to be as high as* 2.2×10^5 m^2/m^3*, which is much higher than those of microchannels (3400–9000* m^2/m^3*) and traditional contactors (50–2050* m^2/m^3*). The artificial neural network model was proposed for predicting* α*, revealing only an average absolute relative error of <5%.* © 2010 American Institute of Chemical Engineers *AIChE J,* 57: 239–249, 2011

Keywords: microporous tube-in-tube microchannel reactor, gas–liquid mass transfer, high interfacial area, high throughput, modeling

Introduction

Gas–liquid contacting is involved in many industrially relevant operations. Among them, gas absorption attracts the most attentions because it is widely applied in the environmental

Correspondence concerning this article should be addressed to J.-F. Chen at chenjf@mail.buct.edu.cn.

protection fields, such as the removal of greenhouse gas CO_2 and hazardous gases of SO_2 and H_2S.[1–4] The conventional gas–liquid contactors used in these processes, including packed tower, spray column, and bubble column, have significant limitations in mass transfer, leading to low efficiency and high cost. Recently, more and more novel reactors with better mass transfer characteristics have been proposed, such as rotating packed bed, external loop gas-lift reactors, spray-tower-loop absorbers, monoliths, and reticulated solid foam packing beds.[5–10]

Microtechnology is an emerging scientific area with great potential application in many industrial processes. The characteristic dimension of micron scale, the extremely large surface-to-volume ratio, and the short transport path in microchannels enhance heat and mass transfer dramatically and hence provide many potential opportunities in chemical process development and intensification.[11] Therefore, in the last 10 years, it has seen the development of microstructured devices for chemical processing such as gas–solid catalytic reactions,[12–14] gas–liquid, and liquid–liquid processes.[15–18] The advantages of them have been demonstrated most impressively.

When gas–liquid processes are performed in microchannels, gas–liquid interfacial areas are expected to be very large, e.g., up to about 20,000 m^2/m^3, which exceeded those of laboratory bubble columns and other conventional industrial gas–liquid contactors by at least one or two orders of magnitude, thus gas–liquid mass transfer rates are greatly increased, which can benefit such applications as gas absorption, gas–liquid catalytic hydrogenation, and direct fluorination.[16,18] However, the maximum throughputs of most reported microreactors, usually at μL or mL/min scale for liquid and at mL/min scale for gas, are much smaller than those of conventional reactors owing to their specific structures, which is hard to meet the demand of industrial applications for high throughput. To obtain a high throughput, a so-called numbering-up method for scale-up of microreactor is mentioned very often.[15,18,19] However, it should be noted that this concept has been, until now, insufficiently implemented from a technical point of view.[11] The most important challenge is how to ensure flow equidistribution with minimal pressure loss in each microchannel.[11,20] Another reason is the high expenditure of fabrication involving numbering-up. Therefore, it is significant and desired that a high-throughput microstructured gas–liquid contactor is developed by the improvement of a microreactor itself to achieve high gas–liquid mass transfer efficiency.

In this study, a high-throughput microporous tube-in-tube microchannel reactor (MTMCR) is first designed and fabricated as a novel gas–liquid contactor. In the reactor, two tubes, an outer tube and an inner tube, are configured coaxially to form an annular microchannel, and micropores in the annular wall of one end of the inner tube are used as the dispersion media. The reactor can be regarded as a combination of many T-type microreactors configured in parallel circumferentially. The gas flowing outward radially through the annular micropores is dispersed into annular gas streams (gas bubbles) and then impinges crosscurrently at high speed with the axial flow of the liquid in the chamber between the inner and outer tubes, thereby it will exhibit enhanced gas–liquid mass transfer efficiency and large throughput capacity. In MTMCR, CO_2 absorption processes as model gas–liquid contact systems are performed experimentally in water, $NaHCO_3/Na_2CO_3$ buffer solution, and NaOH solution, respectively. Gas–liquid mass transfer characteristics in MTMCR including the interfacial area and the liquid-side volumetric mass transfer coefficient are evaluated. The influence of operational conditions is discussed as well. A comparison of mass transfer performance among different gas–liquid contactors is conducted to exhibit the superiority of MTMCR. In addition, the correlations for predicting the interfacial area are proposed.

On the other hand, extensive modeling works on CO_2 adsorption are reported in the literatures.[5,21,22] For example, Guo et al.[23] developed a model describing three types of mass transfer process in a crossflow RPB. Chen et al.[24] proposed a model for ozonation process in RPB to achieve some empirical correlations. The empirical correlations were proposed to predict mass transfer characters of microchannel reactors.[8,15] However, it seems very difficult to adopt the currently available correlation on the interfacial area in gas–liquid flow in MTMCR owing to its complex microporous structures from special manufacture mode, and a new modeling approach of MTMCR needs to be developed.

Artificial neural networks (ANNs) are usually used to model complex nonlinear systems[25,26–31] and appeared to be a good alternative to traditional empirical, phenomenological, or statistical correlations.[25,28,29,32] The ANNs are more powerful and can manipulate nonlinear input/output relationships more successfully than available literature conventional correlations.[33] Recently, the ANNs have also been successfully used in different industrial applications to describe, control, or model complex chemical processes.[25,28,34–39] For example, Iliuta et al.[28] used neural networks to correlate $\tilde{a}$ and $k_L\alpha$ in trickle-bed reactors over wide ranges of industrial operating conditions. Nevertheless, to the best of our knowledge, the use of ANNs for the correlation of gas–liquid mass transfer in microchannel reactor, especially MTMCR, is reported for the first time in this article. The comparison between the model and experimental data indicates that neural network approach is powerful in predicting interfacial area in MTMCR by training a suitable neural network.

Experimental Section

Experimental apparatus and materials

The schematic diagram of the structure and principle of MTMCR is shown in Figure 1. It can be seen that MTMCR consists of same axle dual tubes. A lot of micropores are distributed around the wall near the entrance end of the inner tube. Figures 2a, b illustrate the photographs of MTMCR and micropores section. The microporous section of MTMCR is composed of several layers of metal meshes. Each mesh was weaved with stainless steel wires of a certain diameter. These meshes were assembled layer by layer with the mesh of larger wire diameter on the surface as a protection layer, followed by precalcination, rolling, and calcination at 1280°C for 3 h to obtain the microporous materials. The microporous materials were then rounded and welded to form the annular microporous section of the reactor. Figures 2c, d give SEM images of the front and cross sections of metal meshes, displaying the very complicated microstructure.

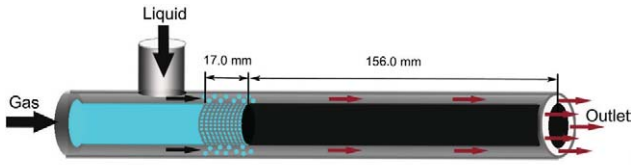

Figure 1. Schematic diagram of microporous tube-in-tube microreactor.

[Color figure can be viewed in the online issue, which is available at wileyonlinelibrary.com.]

In this study, the inner tubes with the pore mean size of 10, 40, 80, 100, and 200 μm are applied, respectively. The widths of mixing chamber between inner tube and outer tube are 250, 500, 750, and 1000 μm, respectively. In addition, the lengths of micropore section and mixing chamber are 17.0 and 156.0 mm, respectively.

Analytical reagent grade sodium hydroxide, hydrochloric acid, sodium carbonate, and sodium bicarbonate were purchased from Beijing Reagent Factory of China. Deionized water was obtained from a water purification system (RO-DI plus, Hitech, PRC). The CO_2 with a purity of 99.5% was bought from Beijing Ruyuanruquan Technology.

The measurement of pressure drop ΔP

A schematic diagram of the test facility for the experiment is presented in Figure 3. The pressure drop ΔP was measured in a H_2O–CO_2 system with a U-type manometer filled with carbon tetrachloride. The U-type manometer was connected just before and after MTMCR. When gas and liquid flowed steadily in MTMCR, the values of ΔP were measured at different superficial gas and liquid velocities.

The process of absorption experiments

The CO_2 absorption experiment with a physical process as an example was performed as followed. Before the experiment, the gas was first fed to the whole system to avoid desorption of CO_2 from the absorption solution. Pure CO_2 from a gas cylinder as the dispersed phase was conveyed by a pressure regulator to the inner tube. Simultaneously, boiled deionized water as the continuous phase was drawn from a liquid tank with a pump. After the high-speed cross-currently impinging with liquid and gas in MTMCR, two-phase mixture flowed downward into a sealed phase separator through a connection tube. Liquid sample for analysis was collected into an excess of NaOH solution at sampling locations 1 and 2, respectively, which were set between MTMCR and the separator, as shown in Figure 3. In addition, the temperatures of gas, liquid, and absorption solution were measured.

The amount of physically absorbed CO_2 was determined by the standard technique of titrating liquid samples with HCl solution. Phenolphthalein and methyl orange were selected as the indicators for the first and second endpoints, respectively. As a blank titration, a similar analysis was also

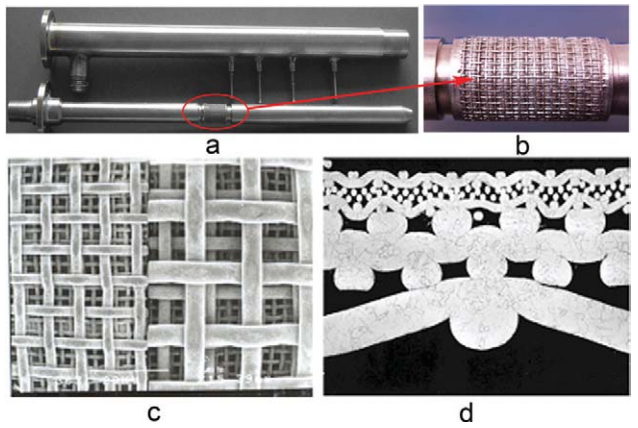

Figure 2. Microporous tube-in-tube microreactor.

(a) The photo of MTMCR, (b) microporous section; SEM images of the front (c) and cross (d) sections of sintering metal wire mesh. [Color figure can be viewed in the online issue, which is available at wileyonlinelibrary.com.]

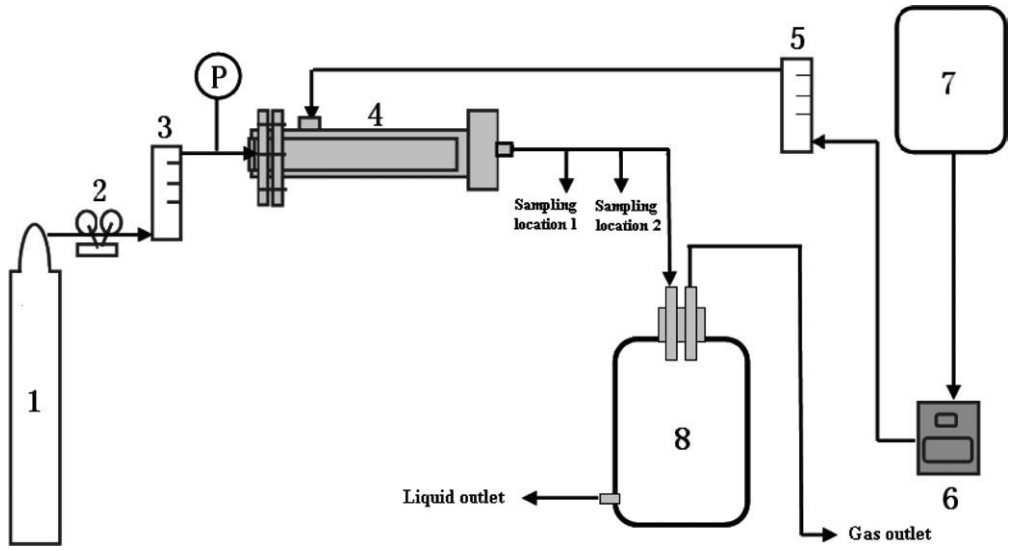

Figure 3. Experimental setup: 1. CO_2 cylinder, 2. pressure regulator, 3. gas flow counter, 4. MTMCR, 5. liquid flow counter, 6. pump, 7. liquid tank, 8. phase separator.

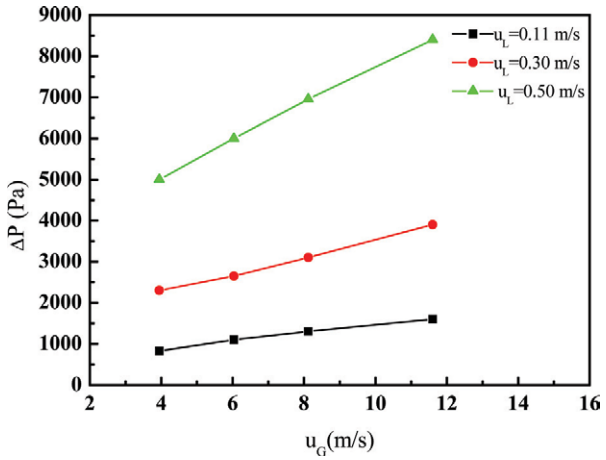

Figure 4. Pressure drop with superficial gas and liquid velocities over MTMCR.

(0.1 MPa, 20°C, R_h = 500 μm, d_h = 10 μm). [Color figure can be viewed in the online issue, which is available at wileyonlinelibrary.com.]

done for the inlet water. The difference provides the amount of CO_2 physically absorbed.

For the chemical absorption process, boiled deionized water was replaced with a buffer solution of 0.3 M $NaHCO_3$/0.3 M Na_2CO_3 or a 1 M NaOH solution. In contrast to physical absorption process, two-phase mixture from the outlet was directly collected by an empty beaker flask without NaOH solution, because there was no risk of CO_2 escape from the alkaline solution into the air. However, the beaker flask should be sealed before the sample was analyzed.

The amount of chemically absorbed CO_2 was calculated from concentration changes in the outgoing solution, which was monitored by titrating liquid samples from the outlet with HCl solution of different concentrations.

The prediction of interfacial area by ANNs model

As an important evaluation parameter for gas–liquid mass transfer, the interfacial area in microchannel is usually expected to be predicted by a reliable and accurate mathematical model. However, the specially complicated micropore structure of MTMCR (Figure 2) would lead to a unique gas–liquid contact behavior and also bring the difficulty to correlate the interfacial area by the conventional model. Interestingly, ANNs have the capability of capturing these dynamics and approximating the behavior of MTMCR under different operating conditions. Therefore, ANNs were here introduced as correlation function for predicting α in this study.

ANNs consist of an input, an output, and one or more hidden layers. Input data supplied to the nodes at the input layer of the ANN and transferred forward through the network to the nodes at the output layer of the ANN. The nodes perform nonlinear input–output transformation by means of a tangent function. Then, the output of the network is compared with the given data, and the weigh and bias are changed to minimize the error between the output values and the data given. Crossvalidation is a technique that can be used to address this problem by iteratively partitioning the sample into two sets of data. One is used for building the model, and the other is used to test it.[40]

In this study, it could be found that the interfacial area values were mainly influenced by several variables, such as micropore size, hydraulic diameter of microannulus, superficial gas and liquid velocities, and liquid and gas densities. A dimensional analysis was performed using these variables, and two dimensionless groups were obtained: Re_G and Re_L.

$$Re_G = \frac{d_h \rho_G u_G}{\mu_G} \tag{1}$$

$$Re_L = \frac{D_h \rho_L u_L}{\mu_L}, \tag{2}$$

where d_h is microporous size, D_h is hydraulic diameter of microannulus and can be expressed as follows:

$$D_h = \frac{4 \times \pi \times [(\frac{D_{outer}}{2})^2 - (\frac{D_{inner}}{2})^2]}{\pi(D_{outer} + D_{inner})} = D_{outer} - D_{inner}. \tag{3}$$

Re_G and Re_L are served as the input parameters, and α is served as the output parameter to build the neural networks model. The experimental data obtained in NaOH–CO_2 absorption process are split into two subsets. 60% of data are used for training the network, whereas the remaining 40% of data are used for testing the network. Furthermore, to evaluate the accuracy of this model, average absolute relative error (AARE) is used as the evaluation criteria. The definition of formula is as follows:

$$AARE = \frac{1}{N}\sum_{1}^{N} \frac{|\alpha_{cal} - \alpha_{exp}|}{\alpha_{exp}}. \tag{4}$$

It should be noted that two phenomena were taken into consideration during the construction and validation of the BPNNs. The first phenomena is overtraining, mainly attributed to a large number of iterations, which generally leads to an excellent prediction of the training data set, while predicting poorly the untrained values. The second phenomenon is undertraining, which interpolates the untaught values relatively well, while predicting poorly the training data set.[41]

Results and Discussion

Pressure drop ΔP

Figure 4 exhibits the evolution of ΔP with superficial gas velocity u_G and superficial liquid velocity u_L, respectively. It could be clearly seen that ΔP increased linearly with increasing u_G at the same u_L. The slopes of these three lines obviously increased with u_L varying from 0.11 to 0.50 m/s. In addition, the change of u_L has a greater effect on ΔP than that of u_G, mainly ascribed to CO_2 absorption in water belonging to a liquid film-controlled process.

Physical absorption experiments

For physical absorption of CO_2 into water, mass transfer is characterized by a mean liquid volumetric mass transfer coefficient, defined according to the following equation:

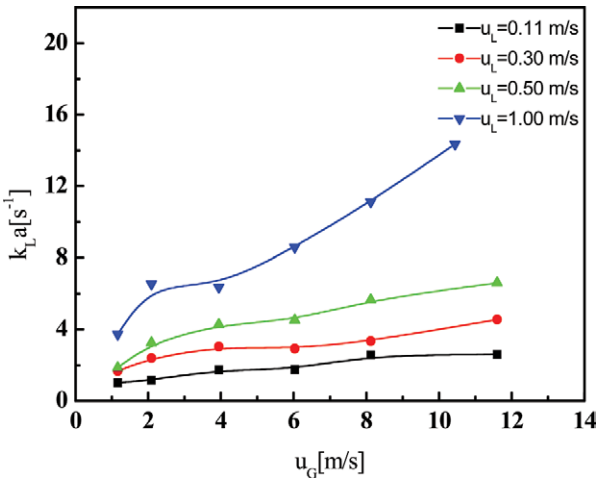

Figure 5. Effect of superficial gas and liquid velocities on liquid side volumetric mass transfer coefficient in MTMCR measured by physical absorption method.

(0.1 MPa, 25°C, $R_h = 500$ μm, $d_h = 10$ μm). [Color figure can be viewed in the online issue, which is available at wileyonlinelibrary.com.]

$$k_L\alpha = \frac{Q_L}{V_{mc}} \ln\left(\frac{C^* - C_{CO_2,0}}{C^* - C_{CO_2,1}}\right). \quad (5)$$

where V_{mc} is the volume of mixing chamber in MTMCR and can be represented as follows

$$V_{mc} = \pi(r_{outer}^2 - r_{inner}^2)L. \quad (6)$$

In our experiments, two sampling locations were positioned after the outlet of MTMCR. As sampling locations 1 and 2 had the same two-phase flow patterns, it could be assumed that the two sampling locations had the same liquid volumetric mass transfer coefficient. That is to say,

$$k_L\alpha_{out,1} = \frac{Q_L}{V_1} \ln\left(\frac{C^* - C_{CO_2,1}}{C^* - C_{CO_2,2}}\right) \quad (7)$$

$$k_L\alpha_{out,2} = \frac{Q_L}{V_2} \ln\left(\frac{C^* - C_{CO_2,2}}{C^* - C_{CO_2,3}}\right) \quad (8)$$

$$k_L\alpha_{out,1} = k_L\alpha_{out,2}. \quad (9)$$

If further, $V_1 = V_2$,

$$\ln\left(\frac{C^* - C_{CO_2,1}}{C^* - C_{CO_2,2}}\right) = \ln\left(\frac{C^* - C_{CO_2,2}}{C^* - C_{CO_2,3}}\right). \quad (10)$$

Thereby, $C_{CO_2,1}$ at the outlet of MTMCR can be accurately obtained and $k_L\alpha$ can be derived by Eq. 5.

Figure 5 plots the measured $k_L\alpha$ in MTMCR as a function of u_L and u_G in CO_2–H_2O physical absorption system. It can be clearly seen that $k_L\alpha$ is significantly increased with the increase of u_L at a fixed u_G. This is mainly ascribed to the fact that increasing u_L would be beneficial to the formation of thinning liquid boundary layer and the corresponding reduction of mass transfer resistance, thereby leading to the increase of k_L. An increase of measured $k_L\alpha$ was also observed when there was an increase in the u_G for a constant u_L. This could be explained by the increase of gas holdup and turbulence of the system.

Liquid side volumetric mass transfer coefficient

For the chemical absorption process, the reaction is said to take place as:[7]

$$CO_2 + CO_3^{2-} + H_2O \rightarrow 2HCO_3^-. \quad (11)$$

According to the experimental results of Roberts and Danckwerts,[55] the apparent first-order rate constant for this reaction, $k_{1,app} = 0.86s^{-1}$. It can be anticipated that when CO_2 is absorbed into the buffer solution in the microchannel contactors under the same ranges of u_L and u_G as those for physical absorption experiments, the following inequality should be fulfilled,

$$k_L\alpha \gg (1-\alpha)k_{1,app}. \quad (12)$$

It means that in the present microchannel contactor, the reaction rate is much slower than the mass transfer rate of CO_2 into the solution, that is to say, the absorption process can be treated as a physical one and CO_2 absorbed remains unreacted in the bulk liquid. Under this condition, the specific rate of absorption can be given by

$$R_{mc} = k_L(C^* - C_{CO_2}). \quad (13)$$

By building a mass balance for dissolved CO_2 in the bulk liquid over an elementary volume and assuming that $k_L\alpha$ is constant, $k_L\alpha$ can be derived as the same as the physical absorption process.

As the same as the physical absorption, there was still gas–liquid contacting in the connection tubes. However, liquid side volumetric mass transfer coefficient here is thought to be very low under the present experimental conditions, and the following inequalities are satisfied.[42–44]

$$(k_L\alpha)_{out} \ll (1-\alpha)k_{1,app} \quad (14)$$

$$k_{L,out}^2 \gg D_{CO_2}k_{1,app}. \quad (15)$$

In this case, the rate of reaction in the diffusion film is negligible, and the concentration of CO_2 in the bulk liquid nears zero. Then, the absorption rate of CO_2 in the outlet region is[45]

$$R_{out} = k_{L,out}C^*. \quad (16)$$

Therefore, a mass balance for $C_{CO_3^{2-}}$ over an elementary volume of the outlet region can be written as

$$-Q_L dC_{CO_3^{2-}} = (k_L\alpha)_{out}C^* dV_{out}. \quad (17)$$

By integrating the above equation, we can derive the average liquid side volumetric mass transfer coefficient in the outlet region as

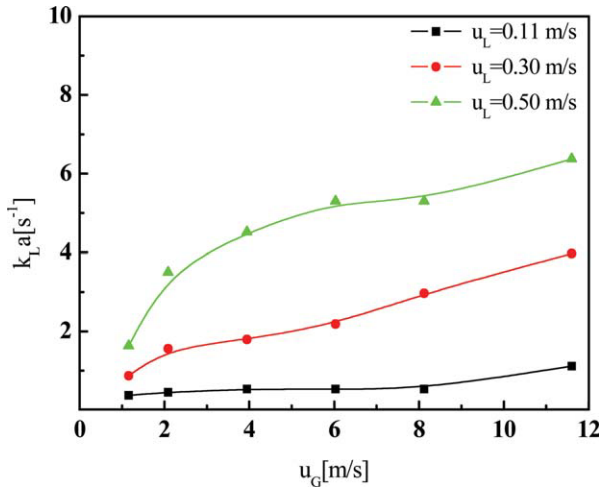

Figure 6. Effect of superficial gas and liquid velocities on liquid side volumetric mass transfer coefficient in MTMCR measured by chemical absorption method.

(0.1 MPa, 25°C, R_h = 500 μm, d_h = 10 μm). [Color figure can be viewed in the online issue, which is available at wileyonlinelibrary.com.]

$$(k_L\alpha)_{out} = \frac{Q_L(C_{CO_3^{2-},0} - C_{CO_2,1} - C_{CO_3^{2-},2})}{C^* V_{out}}. \quad (18)$$

Also, in the tube between sampling locations 1 and 2, $(k_L\alpha)_{out}$ can be expressed as

$$(k_L\alpha)_{out} = \frac{Q_L(C_{CO_3^{2-},2} - C_{CO_3^{2-},3})}{C^* V_{out}}. \quad (19)$$

We could have

$$C_{CO_2,1} = C_{CO_3^{2-},0} - 2C_{CO_3^{2-},2} + C_{CO_3^{2-},3}. \quad (20)$$

From all the above equations, $k_L\alpha$ in MTMCR can be calculated as

$$k_L\alpha = \frac{Q_L}{V_{mc}} \ln\left(\frac{C^* - C_{CO_2,0}}{C^* - C_{CO_3^{2-},0} + 2C_{CO_3^{2-},2} - C_{CO_3^{2-},3}}\right). \quad (21)$$

Figure 6 shows the variation of the measured $k_L\alpha$ in MTMCR with u_L and u_G in the $NaHCO_3/Na_2CO_3$ buffer solution. Clearly, increasing u_L or u_G systematically increases $k_L\alpha$ at a fixed u_G or u_L, which is the same as the change trend in Figure 5. However, the obtained $k_L\alpha$ value by the present chemical method is generally lower than that measured by physical absorption method at the same u_L or u_G. The possible reason is considered to be a lower diffusivity of CO_2 in the buffer solution than that in water.

Interfacial area in MTMCR measured by chemical absorption method

The chemical method based on the absorption of CO_2 into a 1 M NaOH solution[15] was applied to determine the interfacial area in MTMCR. The occurring reaction can be expressed as

$$CO_2 + OH^- \rightarrow HCO_3^- \quad (22)$$

$$HCO_3^- + OH^- \rightarrow CO_3^{2-} + H_2O. \quad (23)$$

As the second reaction is ionic, it takes place at a much faster rate than the first one; therefore, the first reaction step is rate controlling. A general correlation of the second-order rate constant for reaction,[20] k_{OH^-}, was suggested[46]:

$$\lg k_{OH^-} = \lg k^0_{OH^-} + 0.20I - 0.0182I^2 \quad (24)$$

$$\lg k^0_{OH^-} = 13.635 - 2895/T. \quad (25)$$

If the concentration of OH^- remains essentially constant in the bulk of the solution, the equation becomes pseudo-first order. The condition to be satisfied for this is given by the following conditions as suggested by Danckwerts[47]:

$$\sqrt{\frac{D_{CO_2}k_{OH^-}C_{OH^-}}{k_L^2}} \ll 1 + \frac{C_{OH^-}}{2C^*}. \quad (26)$$

That is, CO_2 is entirely consumed in the diffusion film and the interfacial concentration of OH^- is practically the same as that in the bulk liquid phase. Recently, Zanfir et al.[21] have tested this absorption process in a falling film microreactor containing 64 microchannel of 300 μm × 100 μm and found that CO_2 was completely reacted within a very short distance from the gas–liquid interface and the concentration of OH^- did not decrease to zero near the interface, indicating that the limiting step for this reaction occurring in their microreactor is still CO_2 mass transfer in the liquid phase.

It has been shown by Sharma and Danckwerts[48] that the specific rate of absorption per unit area for a second-order reaction satisfying the condition of Eq. 26 is as follows:

$$R = C^*\sqrt{D_{CO_2}k_{OH^-}C_{OH^-} + k_L^2} \quad (27)$$

$$\sqrt{\frac{D_{CO_2}k_{OH^-}C_{OH^-}}{k_L^2}} > 3. \quad (28)$$

The second term within the square root of Eq. 27 becomes small compared with the first term; therefore, the specific rate is given by the simplified equation:

$$R = C^*\sqrt{D_{CO_2}k_{OH^-}C_{OH^-}}. \quad (29)$$

Therefore, the interfacial area in MTMCR is derived as

$$\alpha = \frac{Q_L(\sqrt{C_{OH^-,0}} - \sqrt{C_{OH^-,1}})}{C^* V_{mc}\sqrt{D_{CO_2}k_{OH^-}}}. \quad (30)$$

As to the mass transfer contributions in the outlet region, it is thought that reaction (22) can be considered as instantaneous

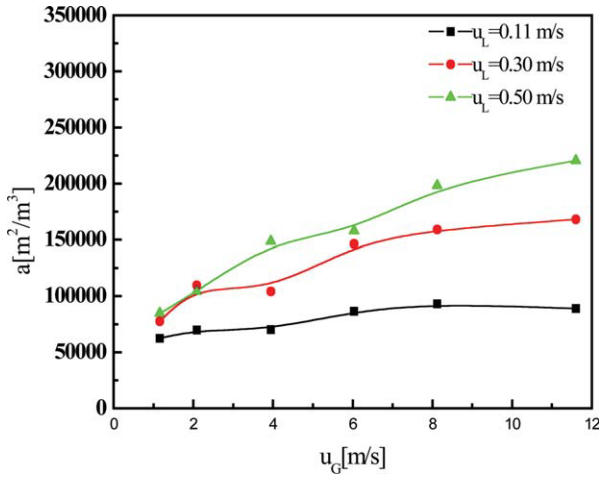

Figure 7. Effect of superficial gas and liquid velocities on interfacial area in MTMCR measured by chemical absorption method.

(0.1 MPa, 25°C, R_h = 500 μm, d_h = 10 μm). [Color figure can be viewed in the online issue, which is available at wileyonlinelibrary.com.]

because of much lower liquid side mass transfer coefficient there.[49,50] In other words, the following criterion is fulfilled[46]:

$$\sqrt{\frac{D_{CO_2}k_{OH^-}C_{OH^-}}{k_{L,out}^2}} \gg \sqrt{\frac{D_{CO_2}}{D_{OH^-}}} + \frac{C_{OH^-}}{2C^*}\sqrt{\frac{D_{OH^-}}{D_{CO_2}}}. \quad (31)$$

Under the present experimental conditions, the following inequality exists

$$\frac{C_{OH^-}D_{OH^-}}{2C^*D_{CO_2}} \gg 1. \quad (32)$$

In this case, the specific rate of absorption is as follows:

$$R_{out} = \frac{k_{L,out}C_{OH^-}}{2}\sqrt{\frac{D_{OH^-}}{D_{CO_2}}}. \quad (33)$$

Therefore, we can deduce the average liquid side volumetric mass transfer coefficient in the outlet region as

$$(k_L\alpha)_{out} = \frac{Q_L}{V_{out}}\sqrt{\frac{D_{OH^-}}{D_{CO_2}}}\ln\left(\frac{C_{CO_2,1}}{C_{CO_2,2}}\right). \quad (34)$$

We can also get

$$(k_L\alpha)_{out} = \frac{Q_L}{V_{out}}\sqrt{\frac{D_{OH^-}}{D_{CO_2}}}\ln\left(\frac{C_{CO_2,2}}{C_{CO_2,3}}\right). \quad (35)$$

From the above two equations, it is obtained that

$$C_{OH^-,1} = \frac{C_{OH^-,2}^2}{C_{OH^-,3}}. \quad (36)$$

The interfacial area in MTMCR can be measured as

$$\alpha = \frac{Q_L}{C^*V_{mc}\sqrt{D_{CO_2}k_{OH^-}}}\left(\sqrt{C_{OH^-,0}} - \sqrt{\frac{C_{OH^-,2}^2}{C_{OH^-,3}}}\right). \quad (37)$$

The effects of u_L and u_G on the measured interfacial area α in MTMCR by CO_2 absorption into NaOH system are presented in Figure 7. For the different three u_L, the interfacial area increases with an increase of u_G. However, the enhancement trend of α becomes markedly large with slightly increasing u_L. Furthermore, as u_L increases from 0.11 to 0.50 m/s, α almost increases by at least onefold throughout the whole u_G range, indicating that the gas–liquid mass transfer process controlled by liquid film becomes significantly enhanced, as the aforementioned discussed. In particular, the achieved maximum interfacial area of MTMCR can reach as high as 2.2 $\times$ 10^5 m^2/m^3, which is over 10 times as much as those of commonly used microchannel reactors.[10] Such a superhigh interfacial area can be attributed to the complex microporous structures from the special manufacture way, which creates the unique gas–liquid contacting mode and distribution. Also, it leads to the high $k_L\alpha$ and excellent gas–liquid mass transfer performance.

Besides u_L and u_G, the structural sizes of MTMCR, the micropore size and the annular channel width, have also important effect on the interfacial area. Figure 8 displays the effect of the micropore size on the interfacial area. The interfacial area was substantially influenced by the micropore size. As the pore size is increased from 10 to 200 μm, the interfacial area is sharply decreased from 8.9 $\times$ 10^4 to 4.5 $\times$ 10^4 m^2/m^3. This is because the bubble size of gas phase as dispersed phase is mainly determined by the micropore size. The smaller is the micropore size, the smaller and the more are the formed gas bubbles. Accordingly, the higher interfacial area is generated.

Figure 9 exhibits the change of the interfacial area with different annular channel widths, another important structure size of MTMCR. It is found that the interfacial area is inversely proportional to the annular channel width. Obviously,

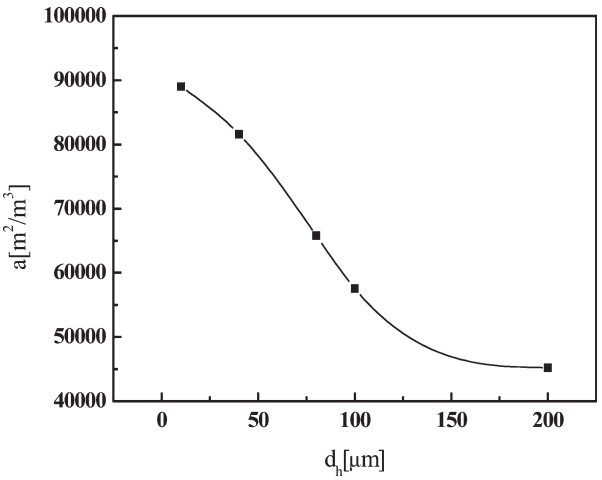

Figure 8. Effect of the micropore size on interfacial area in MTMCR measured by chemical absorption method.

(0.1 MPa, 25°C, R_h = 250 μm, u_L = 0.30 m/s, u_G = 4.64 m/s).

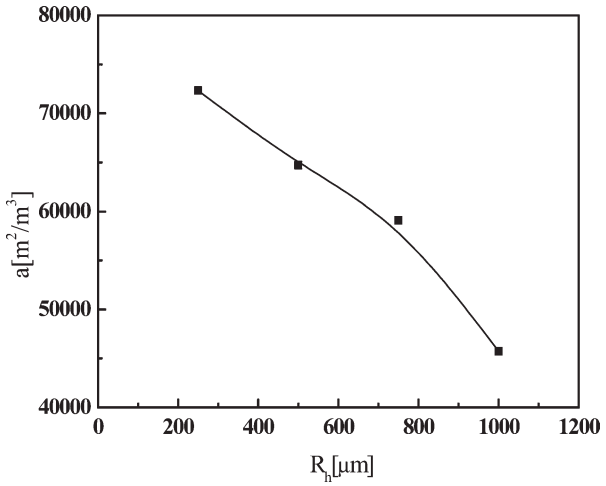

Figure 9. Effect of the annular channel width on interfacial area in MTMCR measured by chemical absorption method.

(0.1 MPa, 25°C, $d_h = 10$ μm, $u_L = 0.30$ m/s, $u_G = 4.64$ m/s).

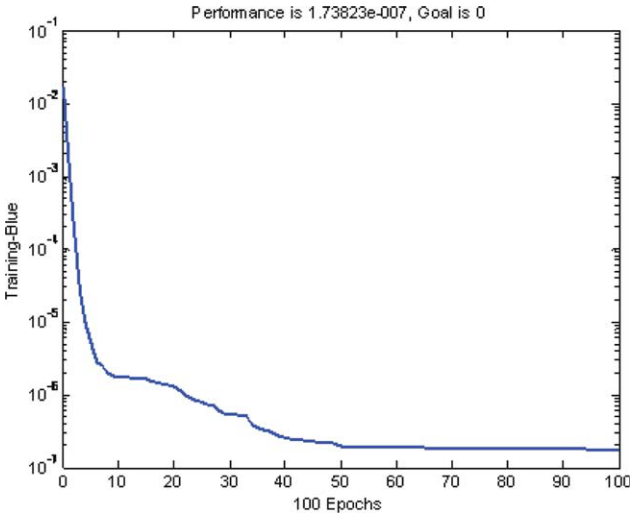

Figure 11. Progress of training.

[Color figure can be viewed in the online issue, which is available at wileyonlinelibrary.com.]

decreasing the annular channel width from 1000 to 250 μm systematically increases the interfacial area from 4.6×10^4 to 7.2×10^4 m^2/m^3. This is possibly owing to the decreased thickness of liquid film, the increased u_L and u_G at the same throughput, as well as the subsequent intensification of gas–liquid mass transfer process.

Predictions of α values using ANNs

All the experimental α data points collected were used to build and validate the ANNs correlations. In the model, the training error and AARE were minimized. The neural networks structure was selected based on testing different networks that vary in terms of structure and simulation parameters. The criterion for network structure selection is based on its simplicity, performance, and accuracy of model prediction. The finally selected network was found for a network topology of 2-3-5-1. The structure of the feed forward neural networks for the model is given in Figure 10. The transfer function, which was both used in hidden and output layers, was a log-sigmoid of the form:

$$F(x) = \frac{1}{1 + e^{-x}}. \tag{38}$$

Levenberg–Marquardt algorithm has been used for training the constructed network for predicting interfacial area in MTMCR.

Figure 11 illustrates the progress of training session. As shown in the figure, the training error sensibly decreased with the number of epochs. Furthermore, the weights and bias of trained networks are given in Table 2, and the prediction of α using ANNs is shown in Figure 12. Obviously, there was nonlinear relation among Re_L, Re_G, and α. Some partial fluctuations were observed, probably attributed to the

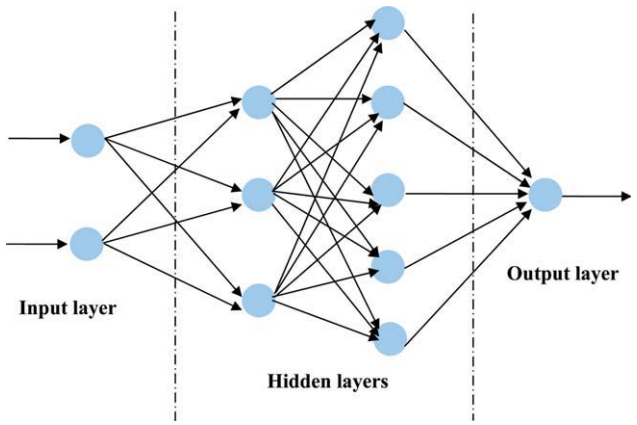

Figure 10. Schematic diagram of the feed forward neural network.

[Color figure can be viewed in the online issue, which is available at wileyonlinelibrary.com.]

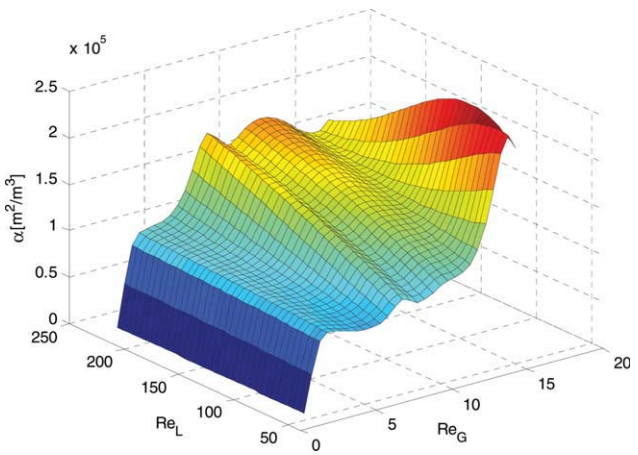

Figure 12. The prediction of α using ANNs.

[Color figure can be viewed in the online issue, which is available at wileyonlinelibrary.com.]

Table 1. Comparison of Mass Transfer Parameters in Different Gas–Liquid Contactors

Type of Contactor	$k_L\alpha$ ($s^{-1} \times 10^2$)	α (m^2/m^3)
Gas–liquid microchannel contactor (1000 μm deep, 500 μm wide)[15]	30–2100	3400–9000
Microporous tube-in-tube microchannel reactor (this work)	100–1435	62,421–220,400
Bubble column[48]	0.5–24	50–600
Impinging jet absorbers[49]	2.5–122	90–2050
Stirred tank[50]	3–40	100–2000
Spray column[50]	1.5–2.2	75–170
Couette-Taylor flow reactor[51]	3–21	700–1200
Static mixers[52]	10–250	100–1000

effect of the complex microporous structures. A comparison analysis was also performed between the experimental data and the calculated data, and the results are given in Figure 13. It can be clearly seen that the results from the trained network show a good agreement with the experimental data. In addition, the AARE is calculated to be 4.67% by the following equation:

$$\mathrm{AARE} = \frac{1}{N}\sum_{1}^{N}\frac{\left|\alpha_{\mathrm{cal}} - \alpha_{\mathrm{exp}}\right|}{\alpha_{\mathrm{exp}}} = 4.67\%. \qquad (39)$$

This result indicates that α in MTMCR can be well predicted by using neural networks with sufficient accuracy. It could be envisioned that the neural network approach is effective for predicting the interfacial area.

Comparison of liquid side volumetric mass transfer coefficient and interfacial area in different gas–liquid reactors

Table 1 gives a comparison of the liquid side volumetric mass transfer coefficient $k_L\alpha$ and the measured interfacial area α of the MTMCR with those of other typical gas–liquid contactors used in the laboratories and industries reported in Refs. [10,21,44–47]. The $k_L\alpha$ and α for conventional batch or semibatch reactors, for example, the packed column or stirred reactor in Table 1, are usually in the range of 0.04–102 or 3–40 and 10–1700 or 100–2000, which means relatively low gas–liquid mass transfer performance. Further, typical microchannel contactor provides a very low throughput and not high α despite its excellent gas–liquid mass transfer performance resulted from high $k_L\alpha$ value of 30–2100. Therefore, from an industrial point of view, not only are excellent gas–liquid mass transfer efficiency and high α needed but also high throughput is very important. MTMCR possesses excellent gas–liquid mass transfer performance because of the high $k_L\alpha$ from the highest α value (2.2×10^5 m^2/m^3) compared with the results reported in the publications, which is 20 times more than that of typical microchannel contactor (400 μm deep, 500 μm wide). Also, MTMCR has a high throughput of 500 L/h for gas and 43.31 L/h for liquid, which is almost 60 times than that of T-type microchannel contactors. By comparison with other typical reactors, the MTMCR has the capacity of accomplishing industrial-scale assignment as well as achieving excellent gas–liquid mass transfer performance. Thus, it could be envisioned that the MTMCR would exhibit great potential for various industrial applications in future, especially for CO_2 capture.

Table 2. Weights and Biases of the 2-3-5-1 Dimensional BPNN

Weights of First Hidden Layer	1	2
1	−0.32	5.1×10^{-3}
2	0.92	3.4×10^{-3}
3	3.37	0

Weights of Second Hidden Layer	1	2	3
1	−4.01	−3.16	−5.35
2	−10.85	−3.32	−2.14
3	−12.23	8.64	−7.85
4	0.55	−7.56	4.59
5	−5.36	−6.71	3.71

Bias of hidden layers	3.95		−7.82		−2.56
	9.22	9.18	4.27	−1.91	−1.87
Output weights	−6.18	−5.64	6.64	1.94	3.71
Bias of output neuron			−3.46		

Conclusions

In this article, MTMCR was first designed and used as a novel gas–liquid contactor. Gas–liquid mass transfer characteristics in MTMCR were investigated by the absorption of CO_2 into water, $NaHCO_3/Na_2CO_3$ buffer solution, and NaOH solution. MTMCR has a high throughput of 500 L/h for gas and 43.31 L/h for liquid under our experimental conditions, which is 60 times higher than that of T-type microchannel contactors. It could be envisioned that MTMCR would exhibit great potential for various industrial application in future. Increasing the gas or liquid flow rate as well as reducing the micropore size and annular channel width can dramatically intensify gas–liquid mass transfer. The liquid side volumetric mass transfer coefficient in MTMCR slightly increases with the large increase of gas velocity, while dramatically increases with the small increase of liquid

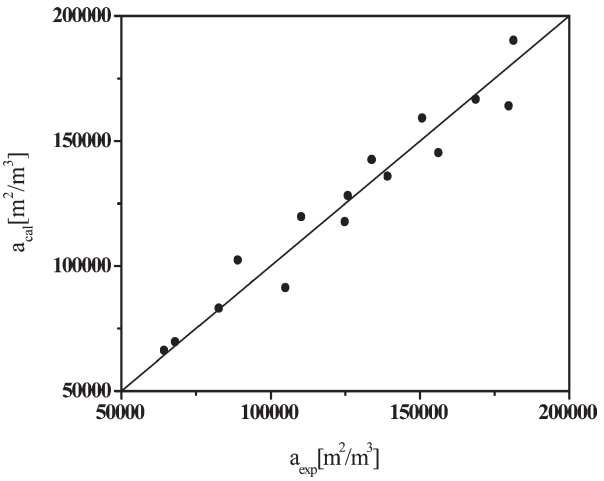

Figure 13. Comparison of predicted and experimental interfacial area values.

velocity. The liquid side volumetric mass transfer coefficient in MTMCR is at least one or two orders of magnitude higher than those in conventional gas–liquid contactors and close to that of typical microchannel reactor. The interfacial area in MTMCR was measured to be as high as 2.2×10^5 m^2/m^3, which is 20 times higher than that in microchannel reactor. The results from a network topology of 2-3-5-1 show a good agreement with the experimental data with a low average relative error of less than 5%, indicating that the neural network approach is effective in predicting interfacial area in MTMCR and lays the foundation for the reactor design.

Acknowledgments

This work was financially supported by National Natural Science Foundation of China (Nos. 20821004, 20990221, and 20806004), National "973" Program of China (No. 2009CB219903), and National "863" Program of China (Nos. 2007AA030207 and 2009AA033301).

Notation

α = interfacial area, m^2/m^3
AARE = average absolute relative error, dimensionless
C_A = molar concentration of component A in the liquid (A = CO_2, HCl, OH^-, HCO_3^-, and CO_3^{2-}), mol/m^3
C^* = physical solubility of CO_2 in the liquid, mol/m^3
D_h = hydraulic diameter of annular tube, m
d_h = hydraulic diameter of micropore, m
D_{CO_2} = diffusivity of CO_2 in the liquid, m^2/s
D_{OH^-} = effective diffusivity of hydroxyl ion in the liquid, m^2/s
I = contribution of an ion in the ionic strength of solution, mol/m^3
u_G = superficial gas velocity, m/s
u_L = superficial liquid velocity, m/s
$k_{1,app}$ = pseudo-first-order rate constant, s^{-1}
k_L = liquid side mass transfer coefficient, m/s
$k_L\alpha$ = liquid side volumetric mass transfer coefficient, s^{-1}
k_{OH^-} = rate constant for reaction between carbon dioxide and hydroxyl ion, $m^3/(mol\ s)$
L = length of the microchannel, m
Q = flow rate, m^3/s
r = diameter of the tube, m
R = rate of absorption per unit interfacial area, $mol/(m^2\ s)$
Re_G = superficial gas Reynolds number defined by $(=d_h u_G \rho_G/\mu_G)$, dimensionless
Re_L = superficial liquid Reynolds number defined by $(=D_h u_L \rho_L/\mu_L)$, dimensionless
T = temperature, K
$V0$ = volume of sample solution, m^3
$V1$ = volume of HCl solution for the first endpoint, m^3
$V2$ = volume of HCl solution for the second endpoint, m^3

Greek letters

α = void fraction
μ = viscosity, Pa s
ρ = density, kg/m^3

Subscripts

0 = inlet of MTMCR
1 = outlet of MTMCR
2 = sampling location 1 of MTMCR
3 = sampling location 2 of MTMCR
cal = the predict data from the model
exp = the experimental data
G = gas phase
inner = the inner tube of MTMCR
L = liquid phase
mc = microchannel section of MTMCR
out = the outlet region of MTMCR
outer = the outer tube of MTMCR

Literature Cited

1. Boucif N, Favre E, Roizard D. CO_2 capture in HFMM contactor with typical amine solutions: a numerical analysis. *Chem Eng Sci.* 2008;63:5375–5385.
2. Delgado JA, Uguina MA, Sotelo JL, Águeda VI, Sanz A. Simulation of CO_2 absorption into aqueous DEA using a hollow fiber membrane contactor: evaluation of contactor performance. *Chem Eng J.* 2009;152:396–405.
3. Nagel D, de Kermadec R, Lintz H, Roizard C, Lapicque F. Absorption of sulfur dioxide in N-formylmorpholine: investigations of the kinetics of the liquid phase reaction. *Chem Eng Sci.* 2002;57:4883–4893.
4. Mandal BP, Bandyopadhyay SS. Simultaneous absorption of carbon dioxide and hydrogen sulfide into aqueous blends of 2-amino-2-methyl-1-propanol and diethanolamine. *Chem Eng Sci.* 2005;60:6438–6451.
5. Yi F, Zou HK, Chu GW, Shao L, Chen JF. Modeling and experimental studies on absorption of CO_2 by Benfield solution in rotating packed bed. *Chem Eng J.* 2009;145:377–384.
6. Mohanty K, Das D, Biswas MN. Mass transfer characteristics of a novel multi-stage external loop airlift reactor. *Chem Eng J.* 2007;133:257–264.
7. Santacesaria E, Seri MD, Iengo P. Mass transfer and kinetics in ethoxylation spray tower loop reactors. *Chem Eng Sci.* 1999;54:1499–1504.
8. Zhang HC, Chen GW, Yue J, Yuan Q. Hydrodynamics and mass transfer of gas-liquid flow in a falling film microreactor. *AIChE J.* 2009;55:1110–1119.
9. Stemmet CP, Bartelds F, van der Schaaf J, Kuster BFM, Schouten JC. Influence of liquid viscosity and surface tension on the gas-liquid mass transfer coefficient for solid foam packings in co-current two-phase flow. Transactions of the Institution of Chemical Engineers. *Chem Eng Res Des.* 2008;86:1094–1106.
10. Stemmet CP, Meeuwse M, van der Schaaf J, Kuster BFM, Schouten JC. Gas-liquid mass transfer and axial dispersion in solid foam packings. *Chem Eng Sci.* 2007;62:5444–5450.
11. Jähnisch K, Hessel V, Löwe H, Baerns M. Chemistry in microstructured reactors. *Angew Chem Int Ed.* 2004;43:406–446.
12. Cao WQ, Chen GW, Li SL, Yuan Q. Methanol-steam reforming over a ZnO-Cr_2O_3/CeO_2-ZrO_2/Al_2O_3 catalyst. *Chem Eng J.* 2006;119:93–98.
13. Ge H, Chen GW, Yuan Q, Li HQ. Gas phase partial oxidation of toluene over modified V_2O_5/TiO_2 catalysts in a microreactor. *Chem Eng J.* 2007;127:39–46.
14. Chen GW, Li SL, Jiao FJ, Yuan Q. Catalytic dehydration of bioethanol to ethylene over TiO_2/c-Al_2O_3 catalysts in microchannel reactors. *Catal Today.* 2007;125:111–119.
15. Yue J, Chen GW, Yuan Q, Luo L, Gonthier Y. Hydrodynamics and mass transfer characteristics in gas-liquid flow through a rectangular microchannel. *Chem Eng Sci.* 2007;62:2096–2108.
16. Hessel V, Angeli P, Gavriilidis A, Löwe H. Gas-liquid and gas-liquid-solid microstructured reactors: contacting principles and applications. *Ind Eng Chem Res.* 2005;44:9750–9769.
17. Zhao YC, Chen GW, Yuan Q. Liquid-liquid two-phase flow patterns in a rectangular microchannel. *AIChE J.* 2006;52:4052–4060.
18. Jähnisch K, Baerns M, Hessel V, Ehrfeld W, Haverkamp V, Löwe H, Wille Ch, Guber A. Direct fluorination of toluene using elemental fluorine in gas/liquid microreactors. *J Fluorine Chem.* 2000;105:117–128.
19. Chambers RD, Fox MA, Holling D, Nakano T, Okazoe T, Sandford G. Elemental fluorine. XVI. Versatile thin-film gas-liquid multi-channel microreactors for effective scale-out. *Lab Chip.* 2005;5:191–198.
20. Tondeur D, Luo L. Design and scaling laws of ramified fluid distributors by the constructal approach. *Chem Eng Sci.* 2004;59:1799–1813.
21. Zanfir M, Gavriilidis A, Wille Ch, Hessel V. Carbon dioxide absorption in a falling film microstructured reactor: experiments and modeling. *Ind Eng Chem Res.* 2005;44:1742–1751.
22. Killion JD, Garimella SA. Critical review of models of coupled heat and mass transfer in falling-film adsorption. *Int J Refrig.* 2001;24:755–797.
23. Guo F, Zheng C, Guo K, Feng YD, Gardner NC. Hydrodynamics and mass transfer in cross-flow rotating packed bed. *Chem Eng Sci.* 1997;52:3853–3859.

24. Chen YH, Chang CY, Su WL, Chen CC, Chiu CY, Yu YH, Chiang PC, Chiang SIM. Modeling ozone contacting process in a rotating packed bed. *Ind Eng Chem Res.* 2004;43:228–236.
25. Yang H, Fang BS, Reuss M. k_La correlation established on the basis of a neural network model. *Can J Chem Eng.* 1999;77:838–843.
26. Hussain MA. Review of the applications of neural networks in chemical process control-simulation and online implementation. *Art Intel Eng.* 1999;13:55–68.
27. Fullana M, Trabelsi F, Recasens F. Use of neural net computing for statistical and kinetic modeling and simulation of supercritical fluid extractors. *Chem Eng Sci.* 2000;55:79–95.
28. Iliuta I, Larachi F, Grandjean BPA, Wild G. Gas-liquid interfacial mass transfer in trickle-bed reactors: state of the art correlations. *Chem Eng Sci.* 1999;54:5633–5645.
29. Larachi F, Iliuta I, Rival O, Grandjean BPA. Prediction of minimum fluidization velocity in three-phase fluidized-bed reactors. *Ind Eng Chem Res.* 2000;39:563–572.
30. Leib TM, Mills PL, Lerou JJ, Turner JR. Evaluation of neural networks for simulation of three-phase bubble column reactors. *Trans IChemE.* 1995;73:690–696.
31. Thibault J, Grandjean BPA. A neural network methodology for heat transfer data analysis. *J Heat Mass Transfer.* 1991;34:2063–2070.
32. Reisener J, Reuter MA, Krüger J. Modeling of the mass transfer in gas-sparged electrolysers with neural networks. *Chem Eng Sci.* 1993;48:1089–1101.
33. Fausset L.*Fundamentals of Neural Networks: Architectures, Algorithms and Applications*.Englewood Cliffs, NJ: Prentice Hall, 1994.
34. Alvarez E, Correa JM, Riverol C, Navaza JM. Model based in neural networks for the prediction of the mass transfer coefficients in bubble columns: study in Newtonian and non-Newtonian fluids. *Int Commun Heat Mass Transfer.* 2000;27:93–98.
35. García-Ochoa F, Gómez Castro E. Estimation of oxygen mass transfer coefficient in stirred tank reactors using artificial neural networks. *Enz Micro Tech.* 2001;28:560–569.
36. Mills PM, Zomaya AY, Tade MO. Adaptive model-based control using neural networks. *Int J Control.* 1994;60:1163–1192.
37. Nascimento CAO, Giudici R. Neural network based approach for optimization applied to an industrial nylon-6,6 polymerization process. *Comp Chem Eng.* 1998;22:595–600.
38. Nascimento CAO, Giudici R, Guardani R. Neural network based approach for optimization of industrial chemical processes. *Comp Chem Eng.* 2000;24:2303–2314.
39. Nikravesh M, Farrell AE, Stanford TG. Control of nonisothermal CSTR with time varying parameters via dynamic neural network control (DNNC). *Chem Eng J.* 2000;76:1–16.
40. Martinez VL, Martinez AR .*Computational Statistics Handbook with MATLAB.* Boca Raton, FL: Chapman & Hall/CRC, 2002.
41. Lemoine R, Fillion B, Behkish A, Smith AE, Morsi BI. Prediction of the gas-liquid volumetric mass transfer coefficients in surface-aeration and gas-inducing reactors using neural networks. *Chem Eng Process.* 2003;42:621–643.
42. Kasturi G, Stepanek JB. Two-phase flow-IV. Gas and liquid side mass transfer coefficients. *Chem Eng Sci.* 1974;29:1849–1856.
43. Shilimkan RV, Stepanek JB. Effect of tube size on liquid side mass transfer in cocurrent gas-liquid upward flow. *Chem Eng Sci.* 1977;32:1397–1400.
44. Tortopidis P, Bontozoglou V. Mass transfer in gas-liquid flow in small-diameter tubes. *Chem Eng Sci.* 1997;52:2231–2237.
45. Danckwerts PV.*Gas-Liquid Reactions*.New York: McGraw-Hill, 1970.
46. Hikita H, Asai S, Takatsuka T. Absorption of carbon dioxide into aqueous sodium hydroxide and sodium carbonate-bicarbonate solutions. *Chem Eng J.* 1976;11:123–129.
47. Danckwerts PV. *Gas-Liquid Reactions.* New York: McGraw-Hill, 1970: 17–20, 97–205.
48. Sharma MM, Danckwerts PV. Chemical methods of measuring interfacial areas and mass transfer coefficients in two fluid systems. *Br Chem Eng.* 1970;15:522–528.
49. Dlusa E, Wronski S, Ryszczuk T. Interfacial area in gas-liquid Couette-Taylor flow reactor. *Exp Therm Fluid Sci.* 2004;28:467–472.
50. Herskowits D, Herskowits V, Stephan K, Tamir A. Characterization of a two-phase impinging jet absorber. II. Absorption with chemical reaction of CO_2 in NaOH solutions. *Chem Eng Sci.* 1990;45:1281–1287.
51. Charpentier JC. Mass-transfer rates in gas-liquid absorbers and reactors. *Adv Chem Eng.* 1981;11:1–133.
52. Kies FK, Benadda B, Otterbein M. Experimental study on mass transfer of a co-current gas-liquid contactor performing under high gas velocities. *Chem Eng Process.* 2004;43:1389–1395.
53. Luo D, Ghiaasiaan SM. Liquid-side interphase mass transfer in cocurrent vertical two-phase channel flows. *Int J Heat Mass Transfer.* 1997;40:641–655.
54. Vandu CO, Liu H, Krishna R. Mass transfer from Taylor bubbles rising in single capillaries. *Chem Eng Sci.* 2005;60:6430–6437.
55. Roberts D, Danckwerts PV. Kinetics of CO_2 absorption in alkaline solutions. I. Transient absorption rates and catalysis by arsenite. *Chem Eng Sci.* 1962;17:961–969.
56. Heyouni A, Roustan M, Do-Quang Z. Hydrodynamics and mass transfer in gas-liquid flow through static mixers. *Chem Eng Sci.* 2002;57:3325–3333.

Manuscript received Sept. 29, 2009, and revision received Mar. 10, 2010.